Polymer 50 (2009) 1908–1917

Contents lists available at ScienceDirect

Polymer

journal homepage: www.elsevier.com/locate/polymer

Smart organic–inorganic nanohybrid stars based on star-shaped poly(acrylic acid) and functional silsesquioxane nanoparticles

Manuela Schumacher [a], Markus Ruppel [a], Joachim Kohlbrecher [b], Markus Burkhardt [a], Felix Plamper [a], Markus Drechsler [a], Axel H.E. Müller [a,*]

[a] Makromolekulare Chemie II and Bayreuther Zentrum für Kolloide und Grenzflächen, Universität Bayreuth, D-95440 Bayreuth, Germany
[b] Laboratory for Neutron Scattering, ETH Zürich & Paul Scherrer Institut, CH-5232 Villigen PSI, Switzerland

ARTICLE INFO

Article history:
Received 25 November 2008
Received in revised form
2 February 2009
Accepted 4 February 2009
Available online 20 February 2009

Keywords:
Polyelectrolyte stars
Poly(acrylic acid)
Hybrids

ABSTRACT

pH- and salinity-responsive organic–inorganic nanohybrid stars based on poly(acrylic acid) (PAA) stars and *N*,*N*-di(2,3-dihydroxypropyl)3-aminopropylfunctional silsesquioxane nanoparticles are readily formed by mixing of aqueous solutions of the components. The interaction between stars of two different arm lengths, $(PAA_{100})_{21}$, $(PAA_{200})_{24}$, with water-soluble silsesquioxane nanoparticles is studied according to changes in pH and salt concentration. The original size of the stars is conserved during complexation according to dynamic light scattering (DLS) measurements and light scattering (LS) titration experiments, which exclude star–star aggregation or crosslinking during the interaction. The proposed interaction mechanism is based on hydrogen-bonding and Coulomb interactions. Cryogenic transmission electron microscopy measurements demonstrate the formation of nanohybrid stars. Small-angle neutron scattering experiments enable a quantitative determination of the fraction of bound nanoparticles and indicate an equilibrium between free and bound nanoparticles.

1. Introduction

Organic–inorganic hybrid materials have found great interest, in particular in the areas of biomaterials, optical and mechanical applications. New materials like those hybrids with unique properties are formed through the combination of organic and inorganic material properties [1–5]. An important class of hybrid materials contains silica or silsesquioxanes as the inorganic component. The organic and inorganic components can be simply mixed, e.g. in nanocomposites [5–14], they can be attached in a covalent way [5,9,10,15–22] or they can form defined complexes [9,10,23–27]. The preparation of polymer–nanoparticle assemblies remains a tedious task. Nanoparticles are commonly not readily miscible with polymers [28,29] due to entropic reasons combined with chain stretching. Only strong enthalpic interactions may overcome the entropic penalty and may promote the mixing of nanoparticles with polymers. One important driving force is Coulombic interaction.

Smart materials, i.e. materials that react on external stimuli like pH, salinity, or temperature offer new applications, in particular sensors, membranes, drug delivery, emulsifiers, foam stabilizers, detergents, nanocontainers, catalysis and biohybrid materials [2–4,30,31]. In particular, weak polyelectrolytes like poly(acrylic acid) (PAA) or poly(*N*,*N*-dimethylaminoethyl methacrylate) (PDMAEMA) have been shown to react by structural and solubility changes on pH, salinity or on the presence of multivalent counterions [3,31–44]. Complexes of weak polyelectrolytes and inorganic materials offer the chance to develop a new class of smart nano-structured organic–inorganic materials [1,2,32].

In various publications we reported the pH-dependent interaction of *N*,*N*-di(2,3-dihydroxypropyl)3-aminopropylfunctional silsesquioxane nanoparticles (Chart 1) with PAA of various topologies. These nanoparticles possess about 14.2 Si atoms and secondary amino functions on average. They have irregular, cage-like structures [45]. Aqueous solution of the nanoparticles and linear PAA showed a pH-dependent turbidity [24,25]. The strongest turbidity was found between pH 2.5 and 5.7. Similarly, planar PAA brushes grafted onto a gold surface showed the strongest interaction at pH = 5.3 [27]. Thus, these nanoparticles penetrate into the PAA brush in the pH range from 5 to 6 but can be liberated at higher or lower pH. Similarly, the interaction of the PAA corona of block copolymer micelles composed of amphiphilic poly(*n*-butyl acrylate)-*block*-poly(acrylic acid) showed a dependence on pH and salinity, the strongest interaction being found at pH ~ 7.5 [26]. We

* Corresponding author. Tel.: +49 921 55 3399; fax: +49 921 55 3393.
E-mail address: axel.mueller@uni-bayreuth.de (A.H.E. Müller).

0032-3861/$ – see front matter © 2009 Elsevier Ltd. All rights reserved.
doi:10.1016/j.polymer.2009.02.010

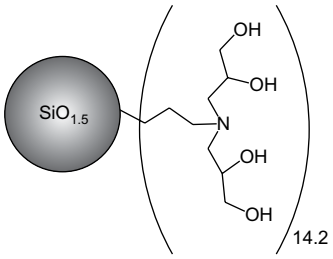

Chart 1. Structure of the used silsesquioxane nanoparticles.

proposed Coulombic and hydrogen-bonding interactions between the acid functions of PAA and the hydroxyl- as well as the amino functions of the nanoparticles. In the case of the interaction with micellar corona it was shown that the nanoparticles have a higher density close to the core of the micelle.

Such interactions resemble the well-known complexation between complementary polymers resulting in the formation of inter-macromolecular complexes stabilized via multisite interactions, either hydrogen-bonding [46,47] or ionic interactions [46,48–50] of complementary units of the coupled polymers. Complexes formed by oppositely charged polyelectrolytes (interpolyelectrolyte complexes, IPECs) precipitate once a certain charge ratio is exceeded [30,42,51–66]. However, in contrast to most IPECs reported in the literature we deal here with two weak polyelectrolytes and the number of ionizable groups in the nanoparticle is rather low (14 tertiary nitrogens).

Polyelectrolyte star polymers containing anionic or cationic hydrophilic arms readily dissolve in water [2,30–32,61,67,68]. In particular, when the arms are weak polyelectrolytes the size of the star depends on pH and salinity. Star polymers may serve as model systems for "frozen" star-like micelles. Interaction of star-shaped PAA having 5–21 arm numbers with a strong cationic polyelectrolyte results in two coexisting populations of complex species, the small ones, forming the major fraction of the mixture, are assumed to represent the water-soluble IPECs. The minor fraction of a large complex species is considered to be aggregates of complexes built through crosslinking of stars by the cationic polyelectrolyte [61].

We were interested in how star-like PAA would interact with the highly functional silsesquioxane particles. These stars have a higher degree of organization than linear PAA. In contrast to dynamic – but kinetically frozen – micelles (with arm lengths from 100 to 300 PAA units and aggregation numbers, $N_{agg} > 200$) they have similar arm lengths (100 and 200 PAA units, respectively) but a fixed, much lower arm number (21–24 arms). The system presented here follows the same simple mixing procedure of two transparent aqueous solutions to yield a nanohybrid system through the complexation of the PAA arms of the star polymer with the inorganic silsesquioxane nanoparticles in aqueous solution.

Upon complexation various morphological changes may occur. The nanoparticles are expected to interact with the PAA chains inside a single star polymer, resulting in a new class of hybrid materials. Thus, the dimensions of the polyelectrolyte star may be altered but the silsesquioxane nanoparticles may also act as crosslinkers for the stars, leading to larger aggregates. This study should provide a deeper insight into the complexation mechanism of IPECs and organic–inorganic nanohybrids under more controlled conditions as micelles. The potential effects on the dimension of the polyelectrolyte shell on the organic–inorganic nanohybrids are investigated as a function of salinity and pH. Thus, this system may act as a model system for the investigation of water-soluble and stimuli-responsive organic–inorganic nanohybrids.

2. Experimental part

2.1. Materials

Millipore water (Milli-Q, deionized water) was freshly taken from the Millipore+ apparatus, equipped with filtration packs QPAK2E (0.5 μm prefilter, macroreticular activated carbon, high purity mixed bed ion exchange resin, Organex polisher). The resistance of the Millipore water was always around 18.2 MΩ, to ensure that all ions were sufficiently removed. NaCl (Riedel de Haën, p.a.) and NaOH platelets (Merck, p.a.) were used as received. HCl (0.1 N) and NaOH (0.1 N) stock solutions were prepared with Millipore water and Titrisol (Merck) stock solutions. *tert*-Butyl acrylate (*t*BA), acetone, ethylacetate, *N*,*N*,*N*′,*N*″,*N*″-pentamethyldiethylenetriamine (PMDETA), CuBr, $CuBr_2$, CaH_2 and CH_2Cl_2 were bought from Aldrich in highest available purity.

The synthesis of the silsesquioxane nanoparticles is a straightforward two-step synthesis. The addition reaction between 2 molecules of glycidol and (3-aminopropyl)triethoxysilane to *N*,*N*-di(2,3-dihydroxypropyl) (3-aminopropyl)triethoxysilane was followed by a hydrofluoric acid catalyzed hydrolytic condensation reaction [24,25,45]. This led to silsesquioxane particles with an average diameter of 3 nm and a calculated cage-like structure of $(R\text{-}SiO_{1.5})_n$ with $n = 12–18$ (number-average $n = 14.2$).

The synthesis and characterization of the star-shaped poly (acrylic acid) (PAA) with 21 arms and a degree of polymerization (DP) of 100 per arm (denoted as $(PAA_{100})_{21}$) via atom transfer radical polymerization (ATRP) of *tert*-butyl acrylate (*t*BA) as a core-first approach using cyclodextrin-based initiator with subsequent acid treatment of the P*t*BA groups to PAA were reported elsewhere [67]. $(PAA_{200})_{24}$ stars were synthesized via a comparable route as the $(PAA_{100})_{21}$ stars, but using an initiator based on the above-mentioned silsesquioxane nanoparticles, the hydroxyl functions of which were reacted with ATRP initiator functions [68]. Details of the synthesis are given in the Supporting information. Whereas the arm number in the first polymer $(PAA_{100})_{21}$ is nearly equal for all polymer molecules [67], the $(PAA_{200})_{24}$ star obtained from the silsesquioxane macroinitiator has a certain arm number distribution, which is reflected in the polydispersity index of 1.4. In addition it contains ca. 10% of 4-arm stars.

2.2. Preparation of solutions

All star stock solutions ($c_{polymer,max} = 5$ g/L) were obtained by the following procedure. The amphiphilic star polymer was dissolved in NaOH solution overnight at room temperature under stirring. The amount of sodium hydroxide was calculated as 10% excess with respect to the COOH groups of the weighed star polymer to ensure complete deprotonation of the PAA. After addition of the desired amount of NaCl the polymer solution was stirred for at least 12 h. Adjustments of the pH were performed by slow addition of 0.1 M HCl solution under stirring. The stock solutions were diluted by addition of Millipore water with the same salt content and pH as the initial stock solution. All solutions of the PAA stars were transparent and exhibited low viscosity.

The transparent silsesquioxane nanoparticle stock solutions were prepared by dissolving the glassy nanoparticles in Millipore water under stirring at room temperature. The required amount of solid NaCl was added after 1 h.

2.3. Preparation of organic–inorganic nanohybrid stars

Complexation was achieved by slow addition of the nanoparticle stock solution to the star solution with the same ionic strength under stirring. All solutions were equilibrated by stirring for at least

12 h at room temperature prior to the measurements. All nanohybrid star solutions were transparent and showed low viscosity.

2.4. Gel permeation chromatography (GPC) measurements

Molecular weight distributions and averages were characterized by conventional GPC and GPC/viscosity using THF as the eluent, at a flow rate of 0.8–1.0 mL per min, at room temperature. For all GPC systems precolumns (5 μm, 100 Å, 5 cm × 0.8 cm diameter) are used to protect the separation columns. A conventional THF-phase GPC system was used to obtain the apparent molecular weights. GPC system I: column set: 5 μm PSS SDV gel, 10^2, 10^3, 10^4, 10^5 Å, 30 cm × 0.8 cm diameter each; injection volume 20 μL of a 2 mg per mL solution; detectors: Waters 410 differential refractometer and Waters 996 photodiode array detector. Narrow PS standards (PSS, Mainz) were used for the calibration of column set I. The molecular weight of the star-shaped polymer was determined by the universal calibration principle [69] using the viscosity module of the PSS WinGPC scientific V 6.1 software package on GPC system II. Linear PMMA standards (PSS, Mainz) were used to construct the universal calibration curve. GPC system II: column set: 5 μm PSS SDV gel, 10^3 Å, 10^5 Å and 10^6 Å, 30 cm × 0.8 cm diameter each; detectors: Shodex RI-71 refractive index detector, Jasco Uvidec-100-III UV-detector ($\lambda = 254$ nm), Viscotek viscosity detector H502B, which needed to be purged extensively before every measurement and on an Agilent HPLC system (1200 series) with four detectors (UV (260 nm), RI, Viscometer, Model 250 (Viscotek), (Columns: PSS SDV, 10^6 Å, 5 μm, 10^5 Å, 5 μm, 10^3 Å, 5 μm)). The extracted number-average molecular mass M_n was used to determine the degree of polymerization $DP_{n,arm}$ of one arm by dividing M_n by the molar mass of the polymer's repeating unit and, for stars, by the initiation sites per initiator molecule (assuming $f_i = 1$). The initiator was taken into account. The third setup was an aqueous GPC (internal standard ethylene glycol; additives: 0.1 M NaN_3, 0.01 M NaH_2PO_4), which validated that the PAA stars were intact both before and after the purification steps. Column set: two 8 μm PL Aquagel-OH columns (mixed and 30 Å), operated at 35 °C. Detector: Bischoff RI-Detector 8110.

2.5. Dynamic light scattering (DLS) measurements

All solutions were filtered three times through nylon filters (13-HV, Millipore, 0.45 μm pore size) prior to the DLS measurements. The filtered star and the corresponding nanohybrid star solutions were allowed to equilibrate at least for 5 h. The filtered nanoparticle solutions equilibrated at least for 2 h prior use. The DLS measurements were conducted in cross-correlation mode using sealed cylindrical scattering cells ($d = 10$ mm) at five different scattering angles (30°, 60°, 90°, 120° and 150°) with the use of an ALV DLS/SLS-SP 5022F equipment consisting of an ALV-SP 125 laser goniometer, an ALV 5000/E correlator, and a HeNe laser with the wavelength ($\lambda = 632.8$ nm). Measurements were repeated three to five times with an accumulation time between 30 and 300 s. The regularized Laplace inversion (CONTIN algorithm) was applied to analyze the obtained autocorrelation functions. Apparent hydrodynamic radii, R_h, were determined using the intensity-weighted distribution of diffusion coefficients and the Stokes–Einstein equation.

2.6. Light scattering (LS) titration

Experiments were performed with an ALV5000 multiple τ digital correlator and an argon ion laser with a wavelength of 514.5 nm. Titrations were performed using a computer-controlled titration setup (Schott) utilizing a home-made software for synchronising the titrator and the DLS apparatus. LS titration measurements were carried out in home-made glass cells consisting of a cylindrical scattering cell connected to a three necked reservoir containing the solution, the stirrer, the pH-electrode (Mettler Toledo) and the titration tube. Sample preparation followed the same protocol as above. Five DLS measurements per titration step were performed at an angle of 90° with accumulation times of 30–90 s. The different titration parameters like stirring speed, stirring time as well as the lag time between consecutive stirring periods (equilibration period) and DLS measurements were optimized to prevent any kinetic effects. About 65–75 titration steps with a 30 μL addition volume per addition step were mostly used for one LS titration experiment. The concentration of the titrant (100 g/L silsesquioxane nanoparticles) was chosen to ensure only minor dilution effects of the polymer solution. However, the dilution was taken into account during the analysis of the data. After addition of nanoparticles the solutions were vigorously stirred for 60 s for each titration step, followed by a lag time of 60 s without stirring to allow subsequent DLS measurements on quiescent solutions. Measurements of the refractive index increment of the polymer solution were performed on a Diffraction Refractometer DnDC2010/620 (PSS) at $\lambda = 620$ nm.

2.7. Cryogenic transmission electron microscopy (cryo-TEM)

Measurements were performed on a Zeiss EM922 EF-TEM (Zeiss NTS GmbH, Oberkochen, Germany) at temperatures around 90 K. The TEM was operated at an acceleration voltage of 200 kV. Zero-loss filtered images ($\Delta E = 0$ eV) were taken under reduced dose conditions (approx. 100–1000 e/nm^2). All images were recorded digitally by a bottom mounted CCD camera system (Ultrascan 1000, Gatan) combined and processed with a digital imaging processing system (Digital Micrograph 3.10 for GMS 1.5, Gatan). To prepare the sample one drop of the aqueous solution was put on a hydrophilized (home-made equipment, Biozentrum Basel) lacey carbon-coated copper grid (Plano GmbH, Wetzlar, Germany), where most of the liquid was removed with blotting paper leaving a thin film stretched over the lacey holes. The specimens were instantly shock vitrified by rapid immersion into liquid ethane cooled at ~90 K by liquid nitrogen in a temperature-controlled freezing unit (Zeiss Cryobox, Zeiss NTS GmbH, Oberkochen, Germany). The temperature was monitored and kept constant in the chamber during the whole sample preparation steps. After freezing a specimen, remaining ethane was removed using blotting paper. The specimen was inserted into a cryo-transfer holder (CT3500, Gatan, München, Germany) and transferred to the TEM instrument. Examinations were carried out at ~90 K. For evaluation of the data the open source programme ImageJ [70] was used. For normalized averaged radially integrated grey-scale analysis (in the following denoted as "grey-scale analysis") the plugins "Radial Profile" and "Radial Profile Extended" were used. The grey-scale analysis had been performed on various cryo-TEM micrographs with the same magnification over 80–170 nanohybrid stars to ensure good statistics. Cryo-TEM micrographs of the pure stars cannot be obtained due to the bad signal to noise ratio.

2.8. Small-angle neutron scattering (SANS) measurements

Samples for SANS experiments were prepared in D_2O and measured in 1 mm or 2 mm quartz cuvettes (Hellma) at room temperature. Measurements were performed using the instrument D11 at the Institut Laue-Langevin (ILL) (Grenoble, France) with a neutron wavelength λ between 6 Å and 8 Å and at sample-to-detector distances of 1.1, 4 and 16 m, which correspond to a scattering vector q of 0.003–0.34 Å^{-1}. The detector sensitivity and the intensity of the primary beam were calibrated with a 1 mm

reference water sample. The obtained data were radially averaged, corrected for detector background, detector dead time, and the scattering from the empty quartz cuvettes. The relative scattering intensities were converted into absolute units using water as a secondary standard and in accordance with standard routines supplied by ILL. The "GRASP" [71] software package was used for data reduction. SANS data were not corrected for the incoherent background mainly resulting from the solute. DCl and NaOD solutions (Deutero GmbH) were diluted with D_2O (Deutero GmbH) to obtain the required concentration.

2.9. Fitting of SANS measurements

All SANS data shown were normalized to the concentration of the star polymer and given in units of cm^2/g. As the number of PAA arms per star is fixed the detectable increase of the forward scattering intensity can be attributed to the incorporation of the silsesquioxane nanoparticle in the star. The relative change in the scattering intensity compared to the unloaded star can thereby be used to determine the number of nanoparticles per star n_{nano}. The forward scattering intensity as observed by SANS, after subtraction of the q-independent incoherent background and q^{-4} dependent background contribution, which was needed to describe the intensity at very small q-values, can then be calculated (see e.g. [72–75]) by

$$I(q = 0) = k[\beta_{core} + N_{star}\beta_{sh}]^2 \quad (1)$$

with k as a scaling constant, β_{core} as the excess scattering intensity of the core, β_{sh} as the excess scattering intensity of a single PAA molecule in the shell and N_{star} as the arm number of the star.

These are the contribution from the core and a contribution from the scattering of the individual PAA chains. k is a scaling constant, which is obtained from the forward scattering of the pure star.

$$k = \frac{I_{pure\ star}(0)}{(\beta_{core} + N_{star}\beta_{PAA})^2} \quad (2)$$

The excess scattering length of the core β_{core} was taken equal to that of the nanoparticles. The error introduced by this is low since the contribution of this scattering length is small compared to the other contributions. The arm number of the star is known to be $N_{star} = 21$.

The excess scattering intensity of the silsesquioxane nanoparticle, $\beta_{1,nano}$, is known to be $\beta_{1,nano} = V_{nano}(\eta_{nano} - \eta_{solv}) =$ 2596 fm with D_2O as solvent ($\eta_{solv} = 6.33 \times 10^{10}\ cm^{-2}$). The same holds for the excess scattering, β_{sh}, of a single PAA molecule in the shell, $\beta_{sh} = \beta_{PAA} = V_{PAA}(\eta_{PAA} - \eta_{solv})$ with $\eta_{PAA} = 1.59 \times 10^{10}\ cm^{-2}$ and $V_{PAA_{100}} = 10.40 \times 10^{-21}\ cm^3$. The value can be calculated from the scattering length density of PAA, η_{PAA}, and from the molecular volume of PAA, V_{PAA}, where η_{solv} is the scattering length density of the solvent. Hence, β_{PAA} results in 4932 fm for the case of PAA_{100}.

For the nanohybrid stars the excess scattering length of the shell increases linearly with the amount of nanoparticles incorporated in the shell. To account for their scattering contribution – the excess scattering of the shell – is assumed to be

$$\begin{aligned}\beta_{sh} &= \beta_{PAA} + \beta_{nano} \\ &= V_{PAA}(\eta_{PAA} - \eta_{solv}) + x_{nano}V_{nano}(\eta_{nano} - \eta_{solv})\end{aligned} \quad (3)$$

where x_{nano} is the average number of silsesquioxane nanoparticles per PAA arm of the star, V_{nano} ($=4.62 \times 10^{-21}\ cm^3$) the volume of a single nanoparticle and η_{nano} its scattering length density with the value of $0.71 \times 10^{10}\ cm^{-2}$. Equations (1)–(3) allow to calculate x_{nano} from the forward scattering by

$$\begin{aligned}x_{nano} &= \frac{\sqrt{\frac{I(0)}{k}} - (\beta_{core} + N_{star}\beta_{PAA})}{N_{star}\beta_{1,nano}} \\ &= \frac{\left(\sqrt{\frac{I(0)}{I_{pure\ star}(0)}} - 1\right)(\beta_{core} + N_{star}\beta_{PAA})}{N_{star}\beta_{1,nano}}\end{aligned} \quad (4)$$

To fit the scattering curves over the whole q-range a model was developed, which is given as Supporting information.

3. Results and discussion

Poly(acrylic acid) (PAA) stars can directly be dissolved in Millipore water containing 1.1 equivalents of NaOH with respect to the carboxylic functions of the PAA, leading to polyelectrolyte star solutions at pH 9. NaCl can be added subsequently. The pH of the star solutions was adjusted by addition of HCl. The silsesquioxane nanoparticles are highly functionalized with an average of 14.2 tertiary amino groups per particle, each amino function bearing four hydroxyl groups. The radius of the nanoparticles ($R = 1.5$ nm) [24,45] in aqueous solutions is still small compared to the size of the stars ($R = 10$–23 nm at pH 9 and 0.1 M NaCl; see below).

For the formation of the water-soluble nanohybrid stars the star solutions were simply mixed at room temperature with an aqueous solution of the silsesquioxane nanoparticles possessing the same salinity as the star solution. The pH of the formed nanohybrid stars was adjusted by addition of HCl solution. The effect of pH and salinity in the system was studied as they were shown earlier to play an important role in the interaction between the nanoparticles and the PAA.

3.1. Dynamic light scattering (DLS) and LS titrations

DLS measurements (Table 1) provide a first insight into the system. LS titration measurements show systematic changes within the star system during the addition of the nanoparticles. Here, star polyelectrolyte solutions were titrated with a solution of nanoparticles using online pH monitoring and simultaneous dynamic and static LS measurements that were performed on quiescent solutions subsequently after each titration step. The titrations were performed up to a relatively high ratio of nanoparticles per acrylic acid unit of the star polymer, $r = n$(nanoparticles)/n(AA), to ensure oversaturation, which might provoke crosslinking of stars. Here we note that DLS (intensity-weighted CONTIN plot, Fig. 1) and cryo-TEM (Fig. 3 indicated by circles) revealed a minor quantity of large aggregates already present in pure star solutions in the case of the $(PAA_{100})_{21}$ star system. In a mass-weighted size distribution the fraction of aggregates is negligible (<0.1%).

In the case of $(PAA_{200})_{24}$ star–star aggregation led to a characteristic broadening of the size distribution as obtained by CONTIN analysis of the DLS correlation function. This broadening (Table 1) may be rationalised considering the insufficient resolution to discriminate between single PAA stars and star–star aggregates

Table 1
Radii of star systems from DLS and from cryo-TEM measurements ($c_{polymer} = 0.5$–1.0 g/L) at pH 9 before addition of silsesquioxane nanoparticles and at a final stoichiometric ratio $r = n$(nanoparticles)/n(AA) = 0.28–0.60.

	c_{NaCl} [mol/L]	$R_{h,z}$ [nm] pure star	$R_{h,z}$ [nm] nanohybrid	$R_{n,TEM}$ nanohybrid
$(PAA_{100})_{21}$	0.1	10 ± 1	12 ± 1	12 ± 1
	0.02	10 ± 1	10 ± 1	–
$(PAA_{200})_{24}$	0.1	23 ± 2 (broad)	14 ± 2 (sharp)	15 ± 1
	0.02	24 ± 3 (broad)	18 ± 1 (broad)	–

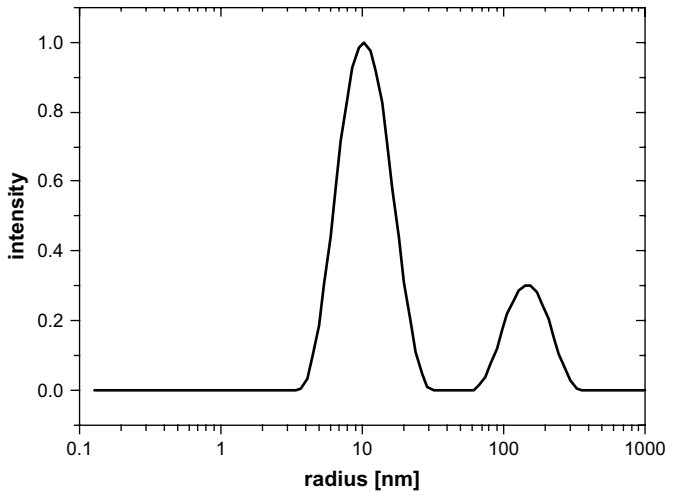

Fig. 1. Typical intensity-weighted CONTIN plot of pure $(PAA_{100})_{21}$ star polymer at pH 5 and 0.1 M NaCl showing the single, well-separated stars and a minor fraction of star–star aggregates (<0.1%).

(with our instrument a factor of 3 in diffusion times is at least required to discriminate different species). Addition of nanoparticles led to sharper distributions as the screening of charges leads to a lower stretching of the PAA arms and hence to a more globular morphology that is in contrast to star–star aggregation [2,31,32,36].

CONTIN analysis of the DLS data of each titration step shows a constant hydrodynamic radius of 10 ± 1 nm in the case of 0.02 M NaCl (Table 1) for the $(PAA_{100})_{21}$ stars and the corresponding nanohybrids. In the case of 0.1 M NaCl (Table 1) the size of the nanohybrids (12 ± 1 nm) is slightly larger than the corresponding pure star (10 ± 1 nm; Fig. 1). Nevertheless, this size change is within the experimental error. The evaluation of the differences between the pure star and the nanohybrid stars was tedious in the case of the $(PAA_{200})_{24}$. As already mentioned the size distribution was broadened (Table 1). Nevertheless, no nanoparticle induced cross-linking of various stars was observed for both star polymers. However, the hydrodynamic radius – as obtained by DLS – is insufficient to provide clear evidence for complexation between the PAA stars and nanoparticles. Here, the discussion of the scattering intensity is more valuable and provides more detailed information.

Fig. 2A (0.1 M NaCl) and C (0.02 M NaCl) shows the LS titration measurement of the $(PAA_{100})_{21}$ star with the nanoparticles. Fig. 2B (0.1 M NaCl) and D (0.02 M NaCl) depicts the same measurement of the larger star $(PAA_{200})_{24}$. The pH increase for all LS titrations is due to the silsesquioxane nanoparticle solution, having an intrinsic pH of 8–9. The polyelectrolyte star solutions were not buffered to eliminate any influence of additional components. All LS titrations (Fig. 2) show a distinct effect in the scattering intensities, measured as the count rates at 90°. The count rate of the star solutions with

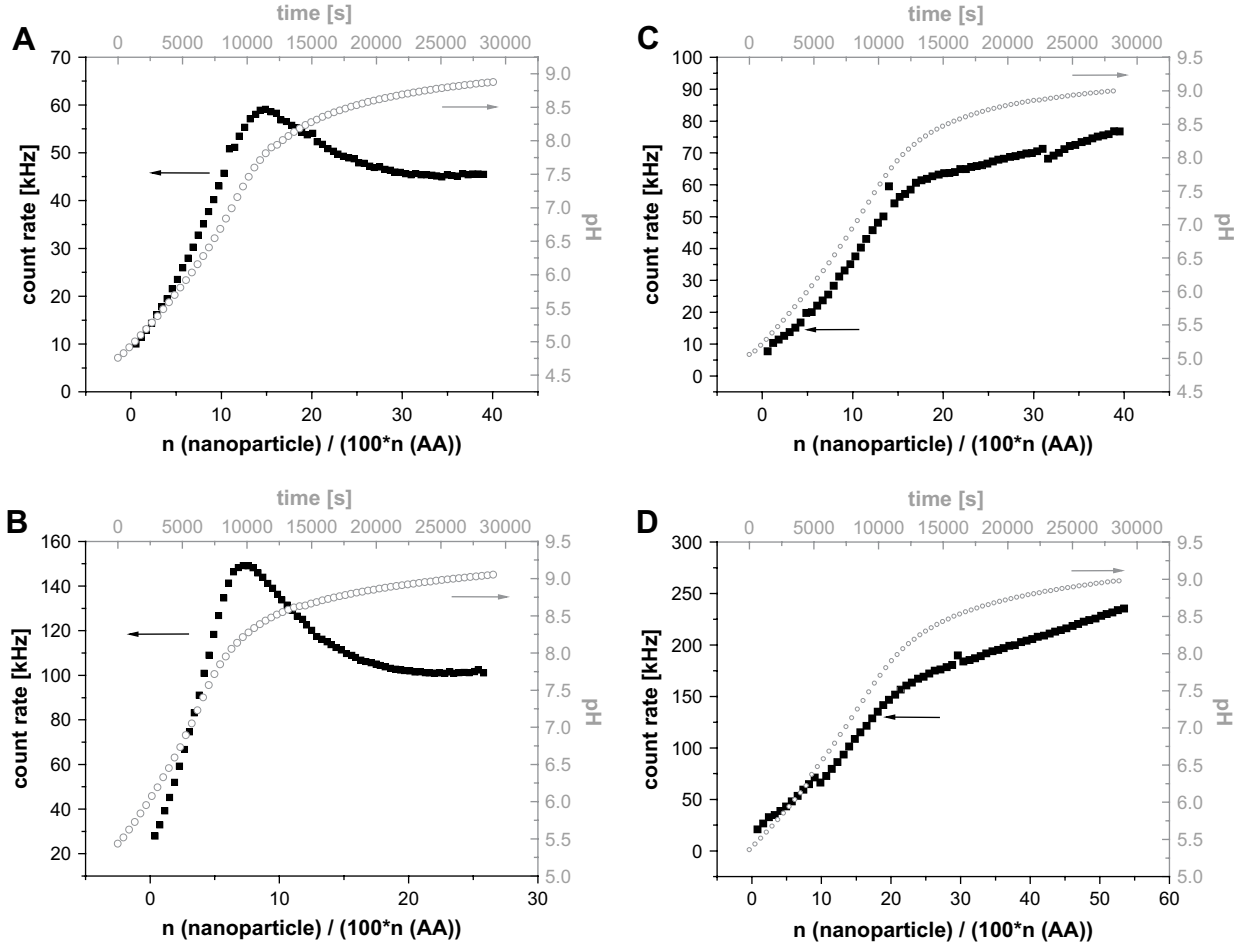

Fig. 2. Light scattering intensities (filled squares) and pH values (open circles) during titration of $(PAA_{100})_{21}$ stars (A: $c_{polymer} = 0.989$ g/L, $c_{NaCl} = 0.1$ M, starting pH 4.76; C: $c_{polymer} = 1.010$ g/L, $c_{NaCl} = 0.02$ M, starting pH 5.06) and $(PAA_{200})_{24}$ (B: $c_{polymer} = 0.958$ g/L, $c_{NaCl} = 0.1$ M, starting pH 5.43; D: $c_{polymer} = 0.942$ g/L, $c_{NaCl} = 0.02$ M, starting pH 5.36) with the silsesquioxane nanoparticles (100 g/L).

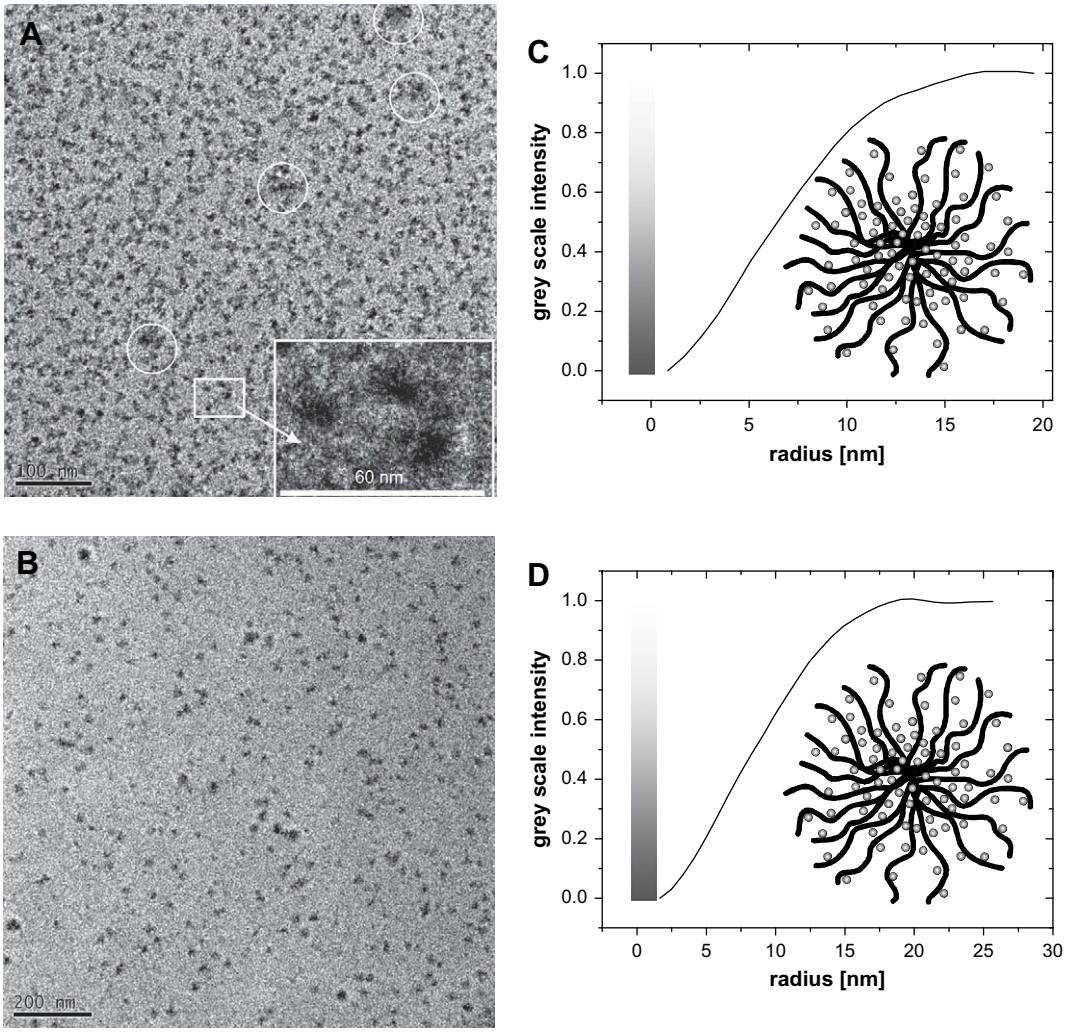

Fig. 3. Cryo-TEM micrographs of nanohybrid stars after LS titration measurements (A: $(PAA_{100})_{21}$; B: $(PAA_{200})_{24}$) without any additional staining at pH 9 and 0.1 M NaCl ($c_{star} \sim 1$ g/L; size bar: A: 100 nm; B: 200 nm) and the corresponding grey-scale analysis (C: $(PAA_{100})_{21}$; D: $(PAA_{200})_{24}$). The circles in A represent star–star aggregates.

a starting pH of around 5 shows a remarkable increase in intensity by a factor of 4–5 for the case of high salinity. In the case of low salinity the effect is even more pronounced with an increased scattering intensity of 10–11. As the count rate depends on the weight concentration, c, and the molecular weight, M_w, of scattering particles and the refractive index increment, dn/dc, and the equipment specific constant K', this increase is a strong indication for the formation of particles with higher molecular weight, i.e. complexation of the stars and silsesquioxane nanoparticles.

$$I = K'c \cdot M_w \left(\frac{dn}{dc}\right)^2 \quad (5)$$

This is true as long as dn/dc of the nanohybrid stars does not increase significantly, the number of the stars stays constant and the pure nanoparticles do not have any significant contribution to the scattering intensity of the solution. The nanoparticles possess a refractive index increment, $dn/dc = 0.150$ mL/g without added salt and of 0.151 mL/g for the solutions with 0.1 M NaCl. Furthermore almost no scattering signal of the pure nanoparticles in solution can be detected because of their low molecular weight ($M_w = 3760$ g/mol). The concentration of the stars and the corresponding nanohybrid stars decrease by 19.5–23.1% of the original value as a result of dilution during titration. The dilution was taken into account for all calculations. The dn/dc values for the polyelectrolyte stars ($(PAA_{100})_{21}$: 0.244 mL/g and $(PAA_{200})_{24}$: 0.197 mL/g) are higher than those of the silsesquioxane nanoparticles. In conclusion, the increased count rate can be only explained by an increased molecular weight, indicating the formation of complexes. The apparent hydrodynamic radii of the stars do not change significantly during complex formation within experimental error (Table 1).

Both star systems with 0.1 M NaCl (Fig. 2A and B) exhibit an increase of the count rate with each titration step until a maximum is reached. A further increase of the nanoparticle concentration leads to gradual decrease of the scattering intensity, which converges to a value 4–5 times higher than the initial scattering intensity. The already mentioned observable second peak (Fig. 1) in the $(PAA_{100})_{21}$ star solutions does not increase during addition of nanoparticles compared to the peak of the pure polyelectrolyte star. The decrease of the count rate starts at pH ~ 8 (0.1 M NaCl, Fig. 2A and B). In the cases of low salinity no maximum is observed (Fig. 2C and D) and the count rate is gradually increasing, reaching a plateau at ca. 10–11 times the initial value. However, a significant change in the slope of the count rate can be detected at pH ~ 8. The absolute scattering intensity is higher than in the case of high ionic strength, because the charges of the polyelectrolyte system with low salt content are less screened. As a result the force to entrap nanoparticles into the PAA star is stronger, leading to nanohybrid stars

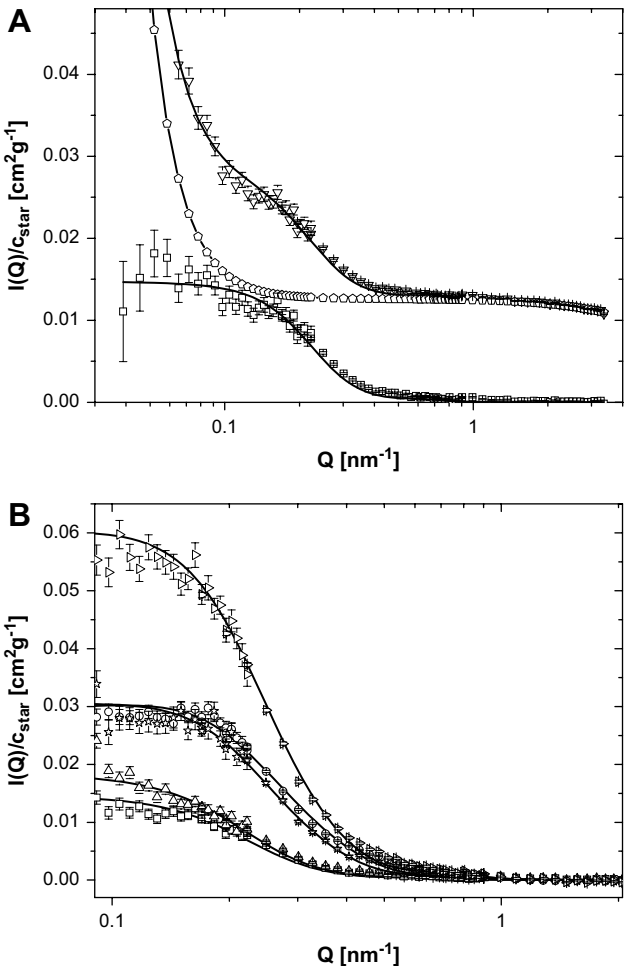

Fig. 4. SANS experimental data and the corresponding fits for $(PAA_{100})_{21}$ star and the respective nanohybrid star at pH 9.5 and 0.1 M NaCl. A (top) shows the experimental data of the pure star (▽), the fitted background (⬠) and the data after background subtraction (□). B (bottom) shows the experimental data after background subtraction with □ as the pure star and all others symbols representing the nanohybrid stars with different content of silsesquioxane nanoparticles in the solution (denotation in Table 2).

with a larger number of interacting nanoparticles and due to that to a higher molecular weight.

This indicates that the interaction between nanoparticles and PAA stars is the strongest for pH < 8 in the case of high salinity. At higher pH the interaction strength weakens, resulting in either a release of nanoparticles at high ionic strength or a diminishing uptake of nanoparticles in the case of low ionic strength. This is in good agreement with the observation that $(PAA_{100})_{21}$ stars with a starting pH > 8 do not show any significant increase in the count rate during the LS titration measurement. Mori et al. [24] found maximum turbidity in the range of pH 2.5–5.7 for linear PAA. Retsch et al. [27] observed a binding maximum at pH = 5.3 for

Table 2
Denotation of the $(PAA_{100})_{21}$ star and the stoichiometry of the mixed solutions of stars and nanoparticles.

Symbol	m_{nano}/m_{star}	n_{nano}/star	$x_{nano,stoich} = n_{nano}$/arm	$r_{stoich} = n_{nano}$/AA unit
□	0	0	0	0
△	2.4	96	4.57	0.046
○	6.1	246	11.6	0.116
☆	12.2	485	23.1	0.231
▷	18.1	717	34.1	0.341

Table 3
Fitted parameters for the $(PAA_{100})_{21}$ star and the corresponding nanohybrid stars at pH 9.5 and 0.1 M NaCl with $\beta_{PAA} = 4932$ fm and $\beta_{1,nano} = 2596$ fm corresponding to the excess scattering length of a single silsesquioxane nanoparticle.

Symbol	β_{nano} [fm]	I_{inc}	10^6 C	$I(Q=0)$ [cm²/g]	x_{nano}	$r_{fit} = x_{nano}$/AA unit	r_{fit}/r_{stoich}
□	0	0.028	0.6	0.014	0	0	
△	755	0.013	0.8	0.019	0.29	0.0029	0.06
○	2269	0.015	1.1	0.029	0.87	0.0087	0.08
☆	2392	0.020	1.1	0.030	0.92	0.0092	0.04
▷	5425	0.022	0.7	0.060	2.09	0.021	0.06

planar PAA brushes, whereas we found strongest interaction for pH < 7.5 for P*n*BA$_{90}$-*b*-PAA$_{300}$ micelles at high salinity [26]. The fact that the stability of IPECs decreases with increasing salinity is well known [61–66]. It indicates that ionic interactions play a significant role in the complexation process.

In conclusion, LS titration measurement revealed a distinct impact of pH and salinity on the interaction strength between PAA stars and nanoparticles. The strongest interactions are present for pH < 7.8, where hydrogen-bonding and Coulomb interactions may be envisaged as main driving forces for complexation. For pH > 8 only ionic interaction or weak hydrogen-bonding interactions may mediate complex formation at intermediate and high pH, respectively. This is sustained by the fact, that an uptake of nanoparticles is maintained at low ionic strength, while a saturation limit is observed at high ionic strength, where Coulomb interactions are known to be effectively screened. This indicates that the degree of ionization of the PAA is a key factor for an effective interaction with the nanoparticles and that hydrogen bonding also plays a vital role [24,25].

3.2. Cryo-TEM

Fig. 3 shows typical cryo-TEM micrographs of the nanohybrid stars (pH 9, 0.1 M NaCl). No staining agent was added. This provides direct evidence for the presence of nanohybrid complexes as the contrast of the pure PAA stars is insufficient to be visible without staining. The evident contrast can be solely attributed to the incorporation of silsesquioxane nanoparticles.

All samples measured by cryo-TEM are solutions after LS titration measurements, i.e. in the presence of a high nanoparticle concentration. Even under these conditions no nanoparticle induced star–star aggregation is evident (Fig. 3A and B). The few larger assemblies in Fig. 3A (circles) are already present in the pure star polymer solutions and are attributed to counterion-mediated star–star aggregation as already mentioned above.

The cryo-TEM micrographs of $(PAA_{100})_{21}$ (Fig. 3A) and $(PAA_{200})_{24}$ (Fig. 3B) clearly prove the uniform distribution of the poly(acrylic acid) nanohybrid stars without significant crosslinking. The single nanohybrid stars exhibit an increased electron and mass density compared to the water background leading to a high contrast (dark spots in the corresponding cryo-TEM micrographs) and they are

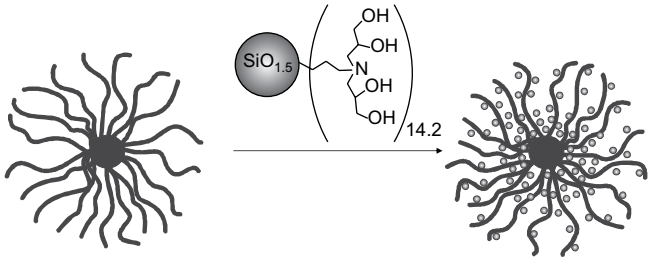

Fig. 5. Formation of organic–inorganic nanohybrid stars.

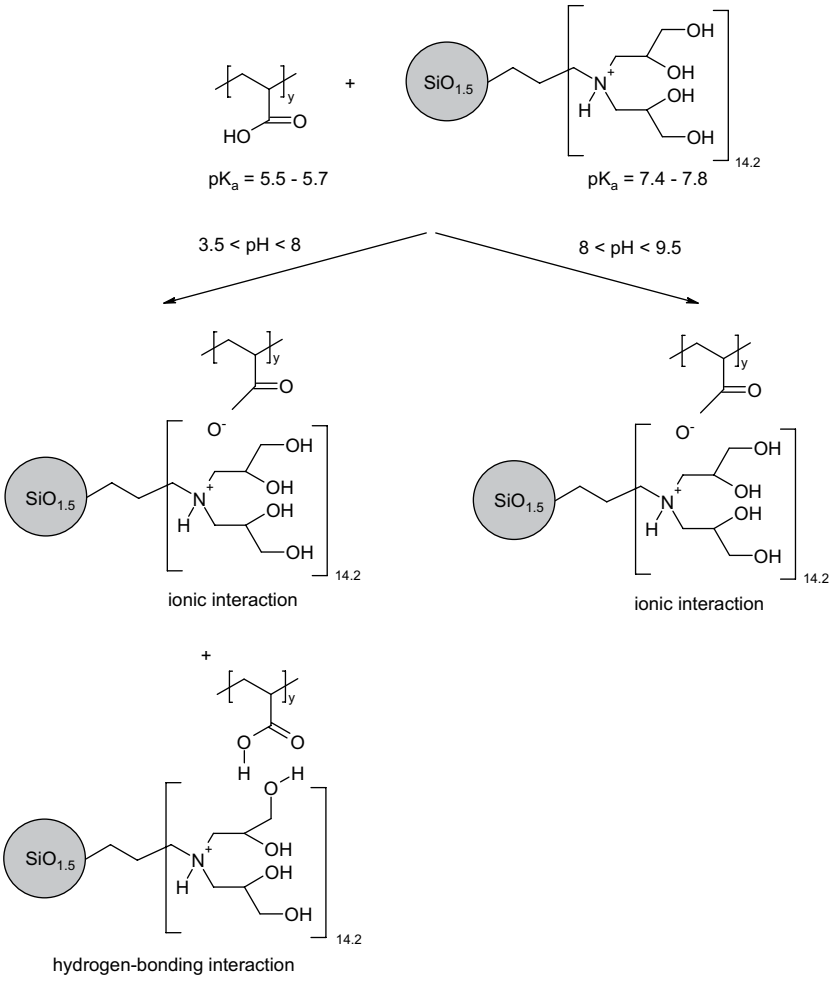

Scheme 1. Potential interaction mechanism between silsesquioxane nanoparticles and PAA of the PAA star.

well separated. The scale bar in the two mentioned micrographs is different (100 nm for $(PAA_{100})_{21}$ in Fig. 3A and 200 nm for $(PAA_{200})_{24}$ in Fig. 3B) due to the different size of the corresponding nanohybrid stars.

The detectable radius of the nanohybrid stars was evaluated by the method of the grey-scale analysis [26]. Here, the high intensity values correspond to low contrast i.e. the lighter parts and vice versa. Thus, the part with an intensity value of 0.0 in the grey-scale analysis corresponds to the PAA–silsesquioxane complex of the nanohybrid star as the data were normalized to be zero for the star centre. The corresponding radial average of the grey-scale intensities is shown in Fig. 3C for the (PAA_{100}) and in Fig. 3D for $(PAA_{200})_{24}$. Both figures illustrate a continuous increase of the grey-scale intensity with increasing distance from the star centre. The radius is deduced at 90% of the total grey-scale intensity, where a distinct change in the slope is evident. For the nanohybrid $(PAA_{100})_{21}$ stars at 0.1 M NaCl (Fig. 3C) we obtain a radius of 12 ± 1 nm which is in good agreement to the DLS measurements of the nanohybrid stars that give a hydrodynamic radius of 12 ± 1 nm (Table 1). The same holds true for the larger PAA star and its corresponding nanohybrids. From Fig. 3D a radius of 15 ± 1.0 nm is evaluated at 90% intensity, close to the hydrodynamic radius.

3.3. SANS experiments

The aim of the SANS measurements was to quantify the amount of nanoparticles within the nanohybrid star. The increase of the forward scattering is a sensitive measure for the amount of silsesquioxane nanoparticles incorporated inside the star. The parameterization for $I(q = 0)$ in Equation (1) has been chosen to account for all constrains determined by the chemical composition of the nanohybrid complexes.

Fig. 4A shows the fitting results (continuous line) together with the experimental data (symbols) of the pure $(PAA_{100})_{21}$ star polymer at pH 9.5 with 0.1 M NaCl. Curve 1 (▽) shows the experimental data and the corresponding fit without background subtraction. Curve 2 (⬠) represents the fitted background, a $I_{inc} + Cq^{-4}$ contribution to the experimental curve. We assume that this contribution is due to the small fraction of star aggregates, which can be described by a q^{-4} power law. Subtraction of the background from the experimental data yields to curve 3 (□). Error bars of each single measurement point are shown.

In Fig. 4B all plots represent experimental data after background subtraction. In addition to the pure star, the experimental scattering functions and the fitting results of the nanohybrid stars with different amount of silsesquioxane nanoparticles is shown. The symbols and the composition of the investigated star–nanoparticle solutions are given in Table 2.

The results of the analysis of the forward scattering are given in Table 3.

The value x_{nano} representing the amount of silsesquioxane nanoparticles within one arm of the star polymer can be divided by the DP of the arms to obtain the number of particles per AA unit, r (Table 3). Those values increase with increasing amount of

nanoparticles in the solution (Table 2). When compared with the stoichiometric quantity we realize that only a fraction of nanoparticles is complexed by $(PAA_{100})_{21}$. This clearly indicates an equilibrium between trapped and free nanoparticles under conditions studied herein. The comparison of the entrapped silsesquioxane nanoparticles with the added amount of nanoparticles to the star solution shows that 4–8% of the added nanoparticles are taking part in the complexation. The remaining nanoparticles stay free in the solution. Consequently, the complexation mechanism must be an equilibrium process, as the addition of more nanoparticles into the polymer solution leads to a higher amount of entrapped nanoparticles within the star at the same pH and salt content shifting the equilibrium towards the side of the organic–inorganic nanohybrid stars.

The quality of the data is not sufficient to provide more precise information about the distribution of the nanoparticles within the star additionally to the information from cryo-TEM that the nanoparticles seem to follow a similar distribution pattern along the PAA chain (Gaussian distribution of the nanoparticles within the PAA star).

The data for the $(PAA_{200})_{24}$ star and its nanohybrids are qualitatively similar, however, the quality of the data is not satisfying for a quantitative evaluation of the incorporated silsesquioxane nanoparticles within the star polymer.

3.4. Proposed interaction model and complexation mechanism

Here we demonstrated the complexation of the nanoparticles and PAA star, which leads to the formation of star-like nanohybrid complexes. Whereas SANS clearly indicates an equilibrium between trapped and free nanoparticles, DLS (Table 1), LS titration (Fig. 2), and cryo-TEM (Fig. 3) do not indicate any crosslinking even at high nanoparticle concentrations. Furthermore, a detailed image analysis of cryo-TEM micrographs (Fig. 3C and D) indicates a linear concentration profile of trapped nanoparticles within the star polymer. Hence, we propose the following morphology for the nanohybrid complexes.

The interaction between silsesquioxane nanoparticles and PAA star polymers is understood to be fully reversible and results in nanohybrid complexes, which are in equilibrium with free nanoparticles in alkaline solution. Cryo-TEM strongly indicates a structure for the nanohybrid complexes, where the density gradually decreases with increasing distance from the centre. The gradual decrease of the nanoparticle number density within the corona is rationalised considering the segment density gradient in the PAA star. The situation is schematically depicted in Fig. 5.

LS titrations (Fig. 2) demonstrate the vital role of two solution properties that affect the complexation: ionic strength and pH. The significant difference in the evolution of the scattering intensity with increasing nanoparticle concentration and pH can be understood considering the main driving forces for complexation: attractive Coulombic interactions and hydrogen bonding between acrylic acid and the hydroxyl groups of the silsesquioxane nanoparticles as shown in Scheme 1 and discussed in detail in our previous paper on the interaction of the nanoparticles with micelles having a PAA corona [26].

4. Conclusions

Mixing aqueous solutions of poly(acrylic acid) PAA stars and silsesquioxane nanoparticles results in the easy and straightforward formation of stimuli-responsive organic–inorganic nanohybrid stars. LS titration measurements provide an insight in the interaction mechanism and show the responsiveness of the system on pH and salinity as external stimuli. Complexation in acidic media is driven by hydrogen-bonding as well as ionic interaction, in alkaline media complexation is solely driven by ionic interaction. Cryo-TEM micrographs confirm the formation of organic–inorganic nanohybrid stars, indicating a gradient in nanoparticle density. This morphology was also sustained by SANS data, which prove the interaction between the silsesquioxane nanoparticles and the PAA, allow for the calculation of the amount of entrapped silsesquioxane nanoparticles within one star.

Acknowledgement

This work was supported by the Deutsche Forschungsgemeinschaft (grant Mu 896/19). Institut Laue-Langevin (ILL, local contact: Ralf Schweins) is gratefully acknowledged for providing SANS beam time and travel support. We thank Jürgen E. Klee (Dentsply DeTrey, Konstanz, Germany), Girish Ch. Behera, Andreas Hanisch and Karina Möller for the preparation of silsesquioxane nanoparticles, Sabine Wunder and Annika Ochs for their help with GPC and titration measurements, Saskia Lindhoud and Remco Fokkink (University of Wageningen, The Netherlands) for their help with the LS titration experiments and programming the LS titration setup, as well as Frank Schubert (University of Bayreuth) for his help with programming the averaging software for DLS measurements. Dmitry V. Pergushov is gratefully acknowledged for helpful comments.

Appendix. Supplementary data

Details of the synthesis of the $(PAA_{200})_{24}$ star. Model for the evaluation of SANS data. This information is available free of charge. Supplementary data associated with this article can be found in the online version, at doi:10.1016/j.polymer.2009.02.010.

References

[1] Kickelbick G. Hybrid materials. Synthesis, characterization and applications. Weinheim: Wiley-VCH; 2007.
[2] Rodríguez-Hernández J, Chécot F, Gnanou Y, Lecommandoux S. Prog Polym Sci 2005;30:691–724.
[3] Riess G. Prog Polym Sci 2003;28:1107–70.
[4] Garnier S, Laschewsky A, Storsberg J. Tenside Surf Det 2003:43.
[5] Hoffmann F, Cornelius M, Morell J, Fröba M. Angew Chem Int Ed 2006;45:3216–51.
[6] Zhao C, Yang X, Wu X, Liu X, Wang X, Lu L. Polym Bull 2008;60:495–505.
[7] Han JT, Xu X, Cho K. Langmuir 2005;21:6662–5.
[8] Wang Y-W, Yen C-T, Chen W-C. Polymer 2005;46:6959–67.
[9] Sanchez C, Julián B, Belleville P, Popall M. J Mater Chem 2005;15:3559–92.
[10] Sanchez C, Soler-Illia GJAA, Ribot F, Lalot T, Mayer CR, Cabuil V. Chem Mater 2001;13:3061–83.
[11] Liu Y-L, Lee H-C. J Polym Sci A 2006;44:4632–43.
[12] Schmid A, Fujii S, Armes SP, Leite CAP, Galembeck F, Minami H, et al. Chem Mater 2007;19:2435–45.
[13] Vaia RA, Maguire JF. Chem Mater 2007;19:2736–51.
[14] Stelzig SH, Klapper M, Müllen K. Adv Mater 2008;20:929–32.
[15] Saito R. J Polym Sci A 2006;44:5174–81.
[16] Du J, Chen Y. Angew Chem 2004;116:5194–7.
[17] Liu Y, Zheng S. J Polym Sci A 2006;44:1168–81.
[18] Alauzun J, Besson E, Mehdi A, Reyé C, Corriu RJP. Chem Mater 2008;20:503–13.
[19] Zhou J, Wang L, Dong X, Yang Q, Wang J, Yu H, et al. Eur Polym J 2007;43:1736–43.
[20] Watanabe M, Tamai T. J Polym Sci A 2006;44:4736–42.
[21] Neouze M-A, Malenovska M, Schubert U, Kotlyar V, Kuperschmidt E, Peled A, et al. J Mater Chem 2008;18:121–5.
[22] Yuan J, Xu Y, Walther A, Bolisetty S, Schumacher M, Schmalz H, et al. Nat Mater 2008;7:718–22.
[23] Ogoshi T, Chujo Y. Macromolecules 2005;38:9110–6.
[24] Mori H, Müller AHE, Klee JE. J Am Chem Soc 2003;125:3712–3.
[25] Mori H, Lanzendörfer MG, Müller AHE, Klee JE. Langmuir 2004;20:1934–44.
[26] Schumacher M, Ruppel M, Yuan J, Schmalz H, Colombani O, Drechsler M, et al. Langmuir, in press. doi:10.1021/la803601a.
[27] Retsch M, Walther A, Loos K, Müller AHE. Langmuir 2008;24:9421–9.
[28] Balazs AC, Emrick T, Russell TP. Science 2006;314:1107–10.
[29] Mackay ME, Tuteja A, Duxbury PM, Hawker CJ, Horn BV, Guan Z, et al. Science 2006;311:1740–3.
[30] Hales K, Pochan DJ. Curr Opin Colloid Interface Sci 2006;11:330–6.

[31] Gil ES, Hudson SM. Prog Polym Sci 2004;29:1173–222.
[32] Förster S, Abetz V, Müller AHE. Adv Polym Sci 2004;166:173–210.
[33] Lazzari M, Liu G, Lecommandoux S. Block copolymers in nanoscience. Weinheim: Wiley-VCH; 2006.
[34] Zhang L, Eisenberg A. Science 1995;268:1728.
[35] Zhang L, Barlow RJ, Eisenberg A. Macromolecules 1995;28:6055–66.
[36] Khougaz K, Astafieva I, Eisenberp A. Macromolecules 1995;28:7135–47.
[37] Gao Z, Varshney SE, Wong S, Eisenberg A. Macromolecules 1994;27:7923–7.
[38] Moffitt M, Khougaz K, Eisenberg A. Acc Chem Res 1996;29:95–102.
[39] Bronich TK, Nguyen HK, Eisenberg A, Kabanov AV. J Am Chem Soc 2000;122:8339–43.
[40] Kabanov AV, Bronich TK, Kabanov VA, Yu K, Eisenberg A. J Am Chem Soc 1998;120:9941–2.
[41] Smitha B, Sridhar S, Khan AA. Macromolecules 2004;37:2233–9.
[42] Petrov AI, Antipov AA, Sukhorukov GB. Macromolecules 2003;36:10079–86.
[43] Sui Z, Jaber JA, Schlenoff JB. Macromolecules 2006;39:8145–52.
[44] Xu Y, Bolisetty S, Drechsler M, Fang B, Yuan J, Harnau L, et al. Soft Matter 2008;8. doi:10.1039/b812179f. Published on the web on October 24.
[45] Mori H, Lanzendörfer MG, Müller AHE, Klee JE. Macromolecules 2004;37:5228–38.
[46] Tsuchida E, Abe K. Adv Polym Sci 1982;45:1.
[47] Kabanov VA, Papisov IM. Vysokomol Soed A 1979;21:243.
[48] Smid J, Fish D. Encyclopedia of polymer science and engineering. New York: Wiley; 1988.
[49] Philipp B, Dautzenberg H, Linow K-J, Koetz J, Dawydoff W. Prog Polym Sci 1989;14:91.
[50] Kabanov VA, editor. Macromolecular complexes in chemistry and biology. Berlin, Heidelberg: Springer; 1994.
[51] Harada A, Kataoka K. J Macromol Sci Part A Pure Appl Chem 1997;A34:2119–33.
[53] Harada A, Kataoka K. Macromolecules 1998;31:288–94.
[54] Harada A, Kataoka K. J Am Chem Soc 1999;121:9241–2.
[55] Harada A, Kataoka K. Science 1999:65–7.
[56] Harada A, Kataoka K. Macromolecules 1995;28:5294–9.
[57] Thünemann AF, Müller M, Dautzenberg H, Joanny J-F, Löwen H. Adv Polym Sci 2004;166:113–71.
[58] Kabanov AV, Kabanov VA. Bioconjug Chem 1995;6:7–20.
[59] Kabanov AV, Vinogradov SV, Suzdaltseva YG, Alakhov VY. Bioconjug Chem 1995;6:639–43.
[60] Kabanov AV, Bronich TK, Kabanov VA, Yu K, Eisenberg A. Macromolecules 1996;29:6797–802.
[61] Pergushov DV, Babin IA, Plamper FA, Zezin AB, Müller AHE. Langmuir 2008;24:6414–9.
[62] Pergushov DV, Remizova EV, Feldthusen J, Zezin AB, Müller AHE, Kabanov VA. J Phys Chem B 2003;107:8093–6.
[63] Pergushov DV, Remizova EV, Gradzielski M, Lindner P, Feldthusen J, Zezina AB, et al. Polymer 2004;45:367–78.
[64] Burkhardt M, Ruppel M, Tea S, Drechsler M, Schweins R, Pergushov DV, et al. Langmuir 2008;24:1769–77.
[65] Lindhoud S, Vries Rd, Norde W, Stuart MAC. Biomacromolecules 2007;8:2219–27.
[66] Hofs B, Keizer Ad, Burgh Svd, Leermakers FAM, Stuart MAC, Millard P-E, et al. Soft Matter 2008;4:1473–82.
[67] Plamper FA, Becker H, Lanzendörfer M, Patel M, Wittemann A, Ballauff M, et al. Macromol Chem Phys 2005;206:1813–25.
[68] Muthukrishnan S, Plamper F, Mori H, Müller AHE. Macromolecules 2005;38:10631–42.
[69] Benoit H, Grubisic Z, Rempp P, Decker D, Zilliox JG. Macromolecules 1966;63:1507.
[70] Rasband WS. U.S. Bethesda, Maryland, USA: National Institutes of Health, http://rsb.info.nih.gov/ij/; 1997–2008.
[71] Dewhurst C. http://www.ill.eu/sites/grasp/grasp_main.html; 2006.
[72] Pedersen JS. J Appl Crystallogr 2000;33:637–40.
[73] Pedersen JS, Svaneborg C. Curr Opin Colloid Interface Sci 2002;7:158–66.
[74] Muller F, Delsanti M, Auvray L, Yang J, Chen YJ, Mays JW, et al. Eur Phys J E 2000;3:45–53.
[75] Förster S, Hermsdorf N, Böttcher C, Lindner P. Macromolecules 2002;35:4096–105.